

Investigating the motility of Ecoli using Fluorescence  
Correlation spectroscopy

Anders Rosengren      Peter Bjødstrup jensen

30 may 2005

# Contents

<b>1</b>	<b>Introduction</b>	<b>2</b>
1.1	E.coli . . . . .	2
<b>2</b>	<b>Theory</b>	<b>4</b>
2.1	Diffusion and random walk . . . . .	4
2.1.1	Fick's law . . . . .	5
2.2	Autocorrelation . . . . .	6
2.2.1	The correlation function . . . . .	6
2.2.2	The analytical form of the correlation function . . . . .	7
2.2.3	Active transport and focus size particles . . . . .	10
2.3	Fluorescence . . . . .	11
<b>3</b>	<b>Experimental setup and methods</b>	<b>13</b>
3.1	Fluorescence Correlation Spectroscopy . . . . .	13
3.1.1	Setup . . . . .	13
3.2	Using rhodamine to determine focal dimensions . . . . .	15
3.3	Growing and preparing bacteria . . . . .	15
3.3.1	Bacterial protocol . . . . .	15
3.3.2	Adjusting the conditions . . . . .	16
3.4	General considerations . . . . .	17
<b>4</b>	<b>Results</b>	<b>18</b>
4.1	Rhodamine measurements . . . . .	18
4.2	Single trace measurements and intensity pattern . . . . .	19
4.3	Fitting procedures and data editing . . . . .	20
4.4	Temperature dependence . . . . .	21
4.5	pH dependence . . . . .	22
4.6	Adhesion & dead bacteria . . . . .	24
4.7	Errors and uncertainties . . . . .	26
4.8	Conclusion . . . . .	28

# Chapter 1

## Introduction

The basis for our investigation of *Escherichia coli* or *E.coli* motility is an experimental method known as Fluorescence Correlation Spectroscopy or FCS. The principle of FCS, is to register and analyze the fluctuations in fluorescence intensity coming from a tiny detection volume in a sample of interest. The means of excitation is a laser, which is strongly focused onto the sample using an objective with a high numerical aperture. This creates detection volumes with dimensions similar to those of an *E.coli* bacterium, i.e. about 1 femtoliter. In the work presented here the assumed 3D ellipsoidal detection volume had a radius  $\approx 400 - 600nm$  and length  $\approx 2500 - 3000nm$  depending on the used objective.

The intensity fluctuations are analyzed using autocorrelation theory, which provides a measure of the self similarity of the fluorescence signal at different times. In order to retrieve meaningful information from the correlated data, a good model for the processes in the sample must be formulated. Very important for the autocorrelation to work properly is very small detection volumes, ensuring low particle density in order for each particle in the focus to contribute significantly to the signal at any one time.

All of these topics will be covered in the coming sections. The FCS setup we are using in our experiments is relatively new, but FCS has been a used experimental procedure since the early 1990'es. The theoretical foundation was introduced in the early 1970'es by Magde, Elson and Webb [1].

The traditional area of application for FCS has been in single molecule experiments, looking at the mobility of proteins or DNA segments, for instance in bacteria. It has so far not been used for studies of the motility of the bacteria itself. Through experiments on *E.coli*'s motility dependency of pH and temperature, this will be the purpose of this study.

### 1.1 *E.coli*

Our test subject, the *E.coli* bacteria, is a single celled cylindrical organism with a double cell membrane, measuring approximately  $1\mu m \times 2\mu m$ . It's means of

propulsion given it has F+ phenotype, as wildtype E.coli does, are multiple flagella extending several cell lengths. A motorcomplex attached in the cell wall generates the torque needed to drive the flagella around, causing them to form a rotating helix behind the bacteria. The viscous forces this generates causes a net movement forward. This is however only when the flagella are rotating counter clockwise, known as the run mode. Rotation clockwise causes E.coli to perform a tumble, which randomly reorients it. Alternating runs and tumbles thus have the bacteria executing a random walk. Depending on conditions, their movement speed is usually found in the range of  $20 - 35 \frac{\mu m}{s}$

In the presence of nutritional or chemical gradients the random walk will be slightly biased towards attractants and away from repellents. This is done by increasing the run time when moving toward attractants. In the absence of gradients, the run and tumble times are approximately 1s and 0.1s respectively. The ability to detect and use chemical gradients to influence movement is known as chemotaxis. It will not be an issue in this experiment, since no such gradients are present.

The source of energy for the rotation of the motor complex, is the free energy stored in a proton gradient or pH gradient across the cytoplasmic membrane of the bacteria. Protons moving along the gradient and crossing the membrane are thought to move or alter the shape of the MotA protein of the motorcomplex and thereby causing the torque needed to rotate the flagella. The protons required to establish and maintain the proton gradient across the membrane, are the result of respiratory processes in the bacteria [2].

The strain of E.coli we have primarily been using for our experiments is E.coli XL1 DsRed. This strain has been genetically modified with the addition of vectors carrying resistance to tetracycline and ampicillin as well as for the production of the red fluorescent protein DsRed. The bacteria produces the protein which is then incorporated into the cell. The presence of this protein is what enables us to detect the bacteria as it passes our focus. The fluorescent properties of the protein are elaborated in Sec.2.3. It is furthermore carrying an F+ factor making it motile. In addition to DsRed, experiments were also made using a strand of E.coli producing green fluorescent protein GFP and one not producing any fluorescent proteins.

The standard approaches to the study of bacterial motility have primarily been the use of 2D or 3D tracking microscopes for directly recording the trajectory of single bacteria, or light scattering techniques. Traditional tracking systems are usually videocameras recording motility tracks through a microscope. In 2D systems restrictions are put on the freedom of movement to ensure that the subject remains in the focal plane. Howard Berg devised the first 3D tracking system for single bacteria in 1971[3], in which the bacteria remained in focus by moving the microscope according to the bacteria. By using two videocameras at a  $90^\circ$  angle, newer tracking microscopes[4] allow the recording of several trajectories simultaneously in three dimensions, and thus improving the statistics.

# Chapter 2

## Theory

### 2.1 Diffusion and random walk

As mentioned previously E.coli, given that they have a F+ factor, will alternate between making runs and tumbles. However when we wish to observe their behavior, we also have to take account for their diffusion/brownian motion. A particle that is freely diffusing, will move due to the kinetic energy it possesses, in average this equals  $\frac{kT}{2}$  in each dimension. Given it is not in vacuum, it will eventually encounter a solvent particle causing it to change direction. The movement of the particle over several encounters with other particles constitutes a random walk. Diffusion can then be defined as the random walk of an ensemble of particles from regions of high concentration to regions of lower concentration.

If we look at a random walk in one dimension ( $\vec{x}$ ) without any external forces, we have a probability that is unbiased and independent of other particles <sup>2</sup>  $p = \frac{1}{2}$  for each particle to go in either direction ( $\pm\vec{x}$ ). They will do so on average for every amount of time  $\tau$  that passes, and travel a distance  $l$  in the  $\pm\vec{x}$  direction, this is considered a step. Lets look at  $N$  particles, we will assume they all start out at time  $t = 0$  and at position  $x = 0$ . After  $n$  steps the  $i$ 'th particle has a position  $x_i(n) = x_i(n-1) \pm l$ , the mean position of the  $N$  particles is then given by:

$$\langle x(n) \rangle = \frac{1}{N} \sum_{i=1}^N x_i(n) \Rightarrow \langle x(n) \rangle = \frac{1}{N} \sum_{i=1}^N (x_i(n-1) \pm l) \quad (2.1)$$

the term  $\pm l$  returns zero when summing due to the equal probability of the two directions, which yields:

$$\frac{1}{N} \sum_{i=1}^N (x_i(n-1)) = \langle x(n-1) \rangle \Rightarrow \langle x(n) \rangle = \langle x(n-1) \rangle \quad (2.2)$$

The mean position of the particles does not change, but they spread. The root mean square displacement  $\langle x^2(n) \rangle^{\frac{1}{2}}$  is easily found going through the same

---

<sup>1</sup> $k$  = Boltzmann's constant;  $T$  the absolute temperature

<sup>2</sup>This assumption is fairly reasonable given that the particles are diluted enough.

steps as above.

$$x_i^2(n) = (x_i(n-1) \pm l)^2 = x_i^2(n-1) \pm 2lx_i(n-1) + l^2$$

$$\Rightarrow \langle x^2(n) \rangle = \frac{1}{N} \sum_{i=1}^N x_i^2(n-1) \pm 2lx_i(n-1) + l^2 = \langle x^2(n-1) \rangle + l^2$$

resulting in:  $\langle x^2(n) \rangle = nl^2$ . Finally expressing  $n$  as a function of time  $n = \frac{t}{\tau}$  and introducing a constant  $D_\tau = \frac{l^2}{2\tau}$  we obtain:  $\langle x^2 \rangle = 2D_\tau t$ . The constant  $D_\tau$  is known as the diffusion constant, a characteristic of the given particles, the medium in which they diffuse and the temperature. Expanded to 3 dimensions we get:

$$\langle (\vec{r}^2) \rangle = 6D_\tau t \quad (2.3)$$

given that the probability also here is independent of other particles and unbiased in each direction ( $\vec{x}, \vec{y}, \vec{z}$ )[5]. The quadratic behavior of Eq.2.3 holds the important difference between diffusion and active transport. Doubling the diffusion distance increases the diffusion time fourfold.

### 2.1.1 Fick's law

In a given time  $dt$ ,

$$dN = -\frac{1}{2}(N(\vec{r} + d\vec{r}) - N(\vec{r}))$$

particles will move a distance  $d\vec{r}$  from  $(\vec{r})$  to  $(\vec{r} + d\vec{r})$  through a surface element  $d\vec{a}$ , resulting in a flux:

$$\vec{J} = \frac{dN}{d\vec{a}dt} = -\frac{1}{2} \left( \frac{N(\vec{r} + d\vec{r})}{dt d\vec{a}} - \frac{N(\vec{r})}{dt d\vec{a}} \right)$$

Multiplying with  $\frac{d\vec{r}^2}{d\vec{r}^2}$ , recognizing  $\frac{dN}{d\vec{a}d\vec{r}}$  as a concentration  $C(\vec{r}, t)$  and the diffusion constant  $D_\tau$  we now have:

$$\vec{J} = -\frac{d\vec{r}^2}{2dt d\vec{r}} \left( \frac{N(\vec{r} + d\vec{r})}{d\vec{a}d\vec{r}} - \frac{N(\vec{r})}{d\vec{a}d\vec{r}} \right) \Rightarrow \vec{J} = -D \frac{1}{d\vec{r}} (C(\vec{r} + d\vec{r}) - C(\vec{r}))$$

Leading us to Fick's 1'st law ( $d\vec{r} \rightarrow 0$ ):

$$\vec{J} = -D_\tau \nabla C \quad (2.4)$$

Now if we use Fick's 1'st law and apply conservation of the total number of particles we end up with Fick's 2'nd law which we'll need later on:

$$\vec{J} = -D_\tau \nabla C \wedge \frac{\partial C}{\partial t} = -\frac{\partial J}{\partial d\vec{r}} \Rightarrow \frac{\partial C}{\partial t} = D_\tau \frac{\partial J^2}{\partial^2 d\vec{r}} = D_\tau \nabla^2 C \quad (2.5)$$

The active selfpropelled transport of E.coli moving through the detection volume, will be taken into account by considering it as being diffusion with drift in Sec.2.2.3. Assuming that the active transport or drift, is the same in all directions, and has the velocity  $v_a$ , fick's 2'nd equation is simply modified to:

$$\frac{\partial C}{\partial t} = D_\tau \nabla^2 C - v_a \nabla C \quad (2.6)$$

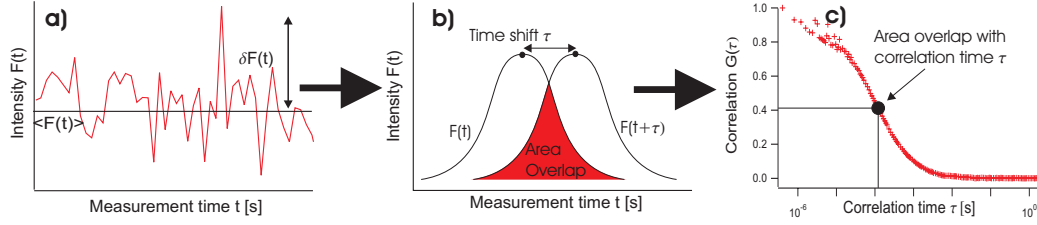


Figure 2.1: The principle of autocorrelation. From intensity signal to correlation curve

## 2.2 Autocorrelation

As bacteria travel through the laser focus, fluorophores are excited and emit photons, creating an ever changing intensity pattern which we register in our photodetectors. (Sec.3.1.1)

Many factors influence the look of the intensity pattern Fig.2.1.a. The amount of background fluorescence sets the ground level, while the peaks from passing bacteria depend on the concentration of bacteria and their conditions, as well as their trajectory through the focus. The way we analyze the intensity pattern to retrieve meaningful information is by using the statistical method of autocorrelation.

### 2.2.1 The correlation function

As the name indicates, correlation theory deals with finding correlated (similar, connected) data in a measured temporal signal. This is done by comparing the intensity signal at time  $t$  to the signal at time  $t+\tau$ . We want to do this over the full length of the signal, to get an average value for the selfsimilarity of the signal, for a given  $\tau$ .

By performing the integral

$$G(\tau) = \frac{1}{T} \int_0^T F(t)F(t + \tau) dt, \quad (2.7)$$

$F(t)$  being the intensity function, over the observation time  $T$ , the value  $G(\tau)$  gives us the correlation value for the given  $\tau$ . To see that this integral gives us a measure of the similarity of the signal at the two times, have a look at Fig.2.1.b. The function  $F(t + \tau)$  corresponds to shifting the entire signal by  $\tau$  to the right. The integral in Eq.2.7 then, is simply the overlap area of the two signals. The larger the overlap, the greater the similarity of the two times. This is the principle of autocorrelation. The overlap can be thought of as representing how much memory the system at time  $t+\tau$  has about the system at time  $t$ . The overlap area visualization however, is only representative if the functions are properly normalized. In standard notation, the right side of Eq.2.7 takes the form  $\langle F(t) \cdot F(t + \tau) \rangle$ . The most obvious way to normalize this would be by using the maximum overlap of the signal, namely  $\langle F(t)^2 \rangle$  which would give  $G(\tau) \in [0; 1]$ .

The actual form of the correlation function however is defined using  $\langle F(t) \rangle^2$  to normalize. This is merely a matter of preference [6].

$$G(\tau) = \frac{\langle F(t) \cdot F(t + \tau) \rangle}{\langle F(t) \rangle^2} \quad (2.8)$$

Since the signal  $F(t)$  can be written as the average signal plus the fluctuations,  $F(t) = \langle F(t) \rangle + \delta F(t)$  and since the average of fluctuations are 0 one gets:

$$\begin{aligned} G(\tau) &= \frac{\langle F(t) \cdot F(t + \tau) \rangle}{\langle F(t) \rangle^2} = \frac{\langle [\langle F(t) \rangle + \delta F(t)] \cdot [\langle F(t) \rangle + \delta F(t + \tau)] \rangle}{\langle F(t) \rangle^2} = \\ &= \frac{\langle F(t) \rangle^2 + \langle \delta F(t) \cdot \delta F(t + \tau) \rangle}{\langle F(t) \rangle^2} = 1 + \frac{\langle \delta F(t) \cdot \delta F(t + \tau) \rangle}{\langle F(t) \rangle^2} \end{aligned} \quad (2.9)$$

Subtracting 1 from Eq.2.9 allows one to look only at the fluctuations in the intensity pattern. By running the calculations simultaneously for all values of  $\tau$  in an interval, one receives a correlation value for each  $\tau$ , ultimately giving a correlation profile Fig.2.1.c. The significant part of the curve, is where it drops from having high correlation to having no correlation. The value of  $\tau$  for which  $G(\tau)$  has halved  $\tau_{\frac{1}{2}}$  tells us something about the average time a fluorescent particle spends in the focus. The higher  $\tau_{\frac{1}{2}}$ , the longer time spend in the focus, corresponding to slower movement.

## 2.2.2 The analytical form of the correlation function

Our goal now, is to arrive at an analytical version of Eq.2.9, providing us with ways to analyze the curve and subtract characteristic coefficients. First we follow the classical approach to this deduction, which is based on point like particles diffusing freely in 3 dimensions. We then add terms taking active transport into account and discuss the problem of application to extended objects.

We make certain assumptions about the intensity signal  $F(t)$ . The signal received by the photo detectors is influenced by many things. Some of these have to do with the spatial distribution of fluorescent events which is directly dependent on the intensity distribution of the laserlight. When the light travels through the pinhole on its way from the sample to the detectors, light originating from decays outside the center of the focal plane, will be cut off to some extent. This is elaborated in Sec3.1.1. This makes for a decaying signal further from the center of the focal plane. The same type of decaying signal is assumed to characterize the intensity signal of the laser light being focused in the sample. These two effects are put together in the term  $I_{em}(\vec{r})$ . Together they define the size of the detection volume from where any light reaches the detectors

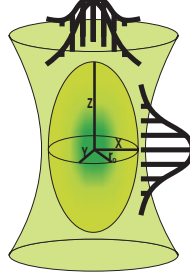


Figure 2.2: The gaussian detection volume

The assumption is now made, that  $I_{em}(\vec{r})$  falls off according to a three-dimensional Gaussian shape when moving away from the center of the focal plane, both in the radial and the axial directions.

$$I_{em}(\vec{r}) = I_0 \cdot \exp\left(-2 \cdot \frac{x^2 + y^2}{r_0^2}\right) \cdot \exp\left(-\frac{2z^2}{z_0^2}\right) \quad (2.10)$$

Here  $r_0$  and  $z_0$  have been introduced, for the distances in radial and axial direction respectively, where the signal has decayed by a factor of  $e^{-2}$ . They define the dimensions of the detection volume. See Fig.2.2. The axial dimension is approximately 5 times larger than the radial. In this report  $z_0$  is not measured directly, but estimated in the range  $2500 - 3000nm$ , depending on the used objective. The values for  $r_0$  will be measured to be in the order of  $400 - 600nm$ .

Other terms are the detection quantum efficiency of the detectors  $q$ , and the excitation cross section of the fluorescent molecule  $\sigma_{abs}$  and their fluorescence quantum yield  $\Phi_f$ . The last two terms are collected in  $Q = \sigma_{abs} \cdot \Phi_f$ . All three are considered constant in time and throughout the detection volume.

The final and most interesting contribution to the final signal comes of course from the immediate concentration of fluorophores in the detection volume  $C(\vec{r}, t)$ .

Putting it all together we arrive at:

$$F(t) = q \cdot Q \int_V I_{em}(\vec{r}) \cdot C(\vec{r}, t) dr^3 \quad (2.11)$$

Since  $I_{em}(\vec{r})$  stays the same if we look at  $\delta F(t)$  instead of  $F(t)$ , we get for  $\delta F(t)$ : (substituting  $\delta C(\vec{r}, t)$  for  $C(\vec{r}, t)$ )

$$\delta F(t) = q \cdot Q \int_V I_{em}(\vec{r}) \cdot \delta C(\vec{r}, t) dr^3 \quad (2.12)$$

Inserting Eq.2.11 and Eq.2.12 into Eq.2.9 we get an expression for the correlation function:

$$G(\tau) = \frac{\int_V \int_{V'} I_{em}(\vec{r}) \cdot I_{em}(\vec{r}') \cdot \langle \delta C(\vec{r}, t) \cdot \delta C(\vec{r}', t + \tau) \rangle dr^3 dr'^3}{(\int_V I_{em}(\vec{r}) \cdot \langle C(\vec{r}, t) \rangle dr^3)^2} \quad (2.13)$$

Assuming freely diffusing particles in three dimensions with diffusion coefficient  $D_\tau$ , the solution to Fick's second equation of diffusion Eq.2.5 can be used to get an expression for the concentration term of Eq.2.13

$$\langle \delta C(\vec{r}, t) \cdot \delta C(\vec{r}', t + \tau) \rangle = \frac{\langle C \rangle}{(4\pi D_\tau \tau)^{\frac{3}{2}}} \cdot \exp\left(-\frac{(\vec{r} - \vec{r}')^2}{4D_\tau \tau}\right) \quad (2.14)$$

We now have expressions for the terms in Eq.2.13, so by substituting Eq.2.10 and Eq.2.14 into Eq.2.13, it can be solved numerically. With a few substitutions the final analytical form of the correlation function for pure diffusion is[7]:

$$G(\tau) = \frac{1}{\langle N \rangle} \cdot \left(\frac{1}{1 + \frac{\tau}{\tau_D}}\right) \cdot \left(\frac{1}{\sqrt{1 + \frac{r_0^2 \tau}{z_0^2 \tau_D}}}\right) \quad (2.15)$$

Here  $\tau_D$  is the mean diffusion time introduced through the formula  $\tau_D = \frac{r_0^2}{4D_\tau}$  already seen in Sec.2.1 for three dimensions Eq.2.3.<sup>3</sup> It is the average time a diffusive particle spends in the detection volume. Also used is the assumption of an elliptical detection volume with volume  $V_{det} = \frac{4}{3}\pi \cdot r_0^2 \cdot z_0$  and  $\langle N \rangle = V_{det} \cdot \langle C \rangle$

With Eq.2.15 one can calculate values for concentration and  $\tau_D$ . The concentration of fluorophores is given simply as the correlation value for  $\tau = 0$

$$G(0) = \frac{1}{N} \quad (2.16)$$

The concentration is thus easily seen from a correlation graph as the reciprocal of the maximum correlation value.

An idea of how to find  $\tau_D$  from the graph can be seen by simplifying Eq.2.15. As already mentioned, the ratio  $\frac{r_0}{z_0}$  is about 1:5. This ratio is squared in the last term of Eq.2.15 making it even smaller. The characteristics of the function is

---

<sup>3</sup>With the 5:1 ratio of  $z_0$  to  $r_0$ , autocorrelation is much more sensitive in the radial direction, justifying the use of only two dimensions.

therefore mainly contained in the first term, making it a good approximation to remove the last term to get:

$$G(\tau) = \frac{1}{\langle N \rangle} \cdot \left( \frac{1}{1 + \frac{\tau}{\tau_D}} \right) \quad (2.17)$$

Isolating  $\tau_D$  in (2.17) and inserting  $\frac{1}{2\langle N \rangle}$  for  $G(\tau_{\frac{1}{2}})$  yields:

$$\tau_D = \frac{\tau_{\frac{1}{2}}}{\frac{1}{\langle N \rangle G(\tau)} - 1} = \frac{\tau_{\frac{1}{2}}}{\frac{2\langle N \rangle}{N} - 1} = \tau_{\frac{1}{2}} \quad (2.18)$$

This means that in the case of pure diffusion,  $\tau_D$  can approximately be found from the correlation graph as the correlation time corresponding to a halving of  $G(\tau)$

### 2.2.3 Active transport and focus size particles

Since Ecoli are not simply freely diffusing particles, but self propelled organisms, Eq.2.15 must be modified to take this into account. Looking at a Ecoli passage of the focus, the active transport of the bacteria can be thought of as diffusion with drift. As seen in Sec.2.1 this involves adding an additional term to Fick's second equation of diffusion which gives Eq.2.6. Using the solutions for this equation, changes the concentration term Eq.2.14 which in turn alters the numerical solution Eq.2.15. One extra term is added yielding:

$$G(\tau) = \frac{1}{\langle N \rangle} \cdot \left( \frac{1}{1 + \frac{\tau}{\tau_D}} \right) \cdot \left( \frac{1}{\sqrt{1 + \frac{r_0^2 \tau}{z_0^2 \tau_D}}} \right) \cdot \exp \left[ - \left( \frac{\tau}{\tau_A} \right)^2 \cdot \left( \frac{1}{1 + \frac{\tau}{\tau_D}} \right) \right] \quad (2.19)$$

Here  $\tau_A$  is the average active transport time spend crossing the detection volume.  $\tau_A = v_a \cdot \langle distance \rangle$  where  $v_a$  is the active transport speed, and  $\langle distance \rangle$  is the mean diameter of the detection volume.

In the limits for pure diffusion  $\tau_A \rightarrow \infty$  and pure active transport  $\tau_D \rightarrow \infty$  we have Eq.2.15 and

$$G_A(\tau) = \frac{1}{N} \cdot \exp \left[ - \left( \frac{\tau}{\tau_A} \right)^2 \right], \quad (2.20)$$

respectively[8]. So the ratio  $\frac{\tau_A}{\tau_D}$  tells whether a given correlation profile is more or less dominated by active transport, compared to that of another correlation profile.

All the autocorrelation theory presented so far is based on conditions with single fluorophore particles much smaller than the size of the focus. The E.coli bacteria is comparable in size to the focus, and we assume that a large number of fluorescent proteins are uniformly distributed in the cell. This probably means that the values returned by Eq.2.19 for  $\tau_D$ ,  $N$  and  $\tau_A$ , when fitting it to an correlation curve, are not accurate. Little work has been done investigating the particle size effect, but one study have shown [9], that for particles with  $\frac{R}{r_0} < 1$ ,  $R$  being the particle radius, a relatively simple modification is valid. The actual diffusion time  $\tau_D$  of an extended particle is simply the diffusion time of an infinitely small point fluorophore  $\tau_{Dinf}$ , increased by the time needed for the particle to diffuse a distance equal to its own radius.

$$\tau_D = \tau_{Dinf} + \frac{R^2}{4D_\tau} \quad (2.21)$$

Since this works as an increase of the apparent detection volume, also the particle number  $N$  is changed.

$$\frac{1}{N} = G(0) = G(0)_{inf} \cdot \left( \frac{1}{1 + \left(\frac{R}{r_0}\right)^2} \right) \quad (2.22)$$

However the study was made in a 2D gaussian, looking at disk shaped particles, and only considering free diffusion, not active transport. It is however reasonable to believe that similar effects occur in our experiments.

A correction term for  $\tau_A$  can therefore probably be constructed similarly, by simply adding the time it would take the bacteria to actively travel a distance similar to its own length. This would be a linear expression involving the active transport velocity  $v_A$ .

$$\tau_A = \tau_{Ainf} + \frac{R}{v_a} \quad (2.23)$$

Here  $\tau_{Ainf}$  is the active transport time of an infinitely small particle. With a radius of about  $1\mu m$  and a velocity of about  $25\frac{\mu m}{s}$  the extra term is in the order 0.04 s

As will be described in Sec.3.1.1 we have used an air objective with only 40X magnification. This produces a larger detection volume than what would normally be considered useful for FCS. However, since E.coli are relatively large, the larger focus will not be a disadvantage.

## 2.3 Fluorescence

As introduced in earlier sections, the principle behind FCS is to observe the self similarity of fluctuations from fluorescent molecules, for instance excited by a laser.

The excited molecule at energy level  $S_1$  can take several courses to it's former energy level, the ground state  $S_0$ . The most likely of these is fluorescence, releasing it's excess energy as a single photon Fig.2.3.a. It can also return to a highly

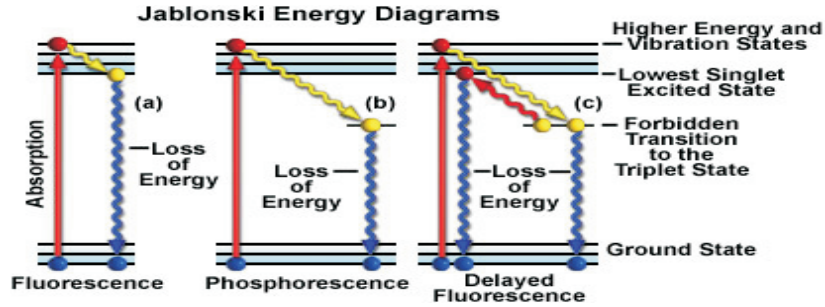


Figure 2.3: The energy diagram for the excitation and emission processes [12]

vibrational ground state, by internal conversion, a path that doesn't directly affect FCS since electrons and not photons are released. It might also go to a triplet state  $T_1$  with an energy below  $S_1$  via inter system crossing which does not radiate, from where it again can take different paths. Amongst these is another energy increase where it obtains another triplet state with a higher energy than that of  $S_1$  to then again return to the  $S_1$  state. By further inter system crossing it can return to a high vibrational  $S_0$  state, again without radiation.

Finally and most importantly it can go from the triplet state to the ground state by phosphorescence also emitting photons Fig.2.3.b. This results in a additional correlation, thus making this effect undesired. [7].

Since the probability of the molecule to obtain the triplet state is a function of the power of which it is excited, using a low effect laser, as is the case for our experiment as seen in a later section, can reduce phosphorescence. This also reduces a phenomena known as bleaching, that a fluorophore only can absorb and emit a photon a limited number of times.

Hence desirable characteristics of a fluorophore would be low phosphorescence yield, low rates of intersystem crossing and internal conversion, but foremost a high quantum yield of fluorescence.

The Fluorescent protein that is introduced in our preferred E.coli variant is known as DsRed. It has to some extent these characteristics, a quantum yield of 0.79, it's excitation spectrum peaks at  $558nm$  and it's emission's at  $583nm$  [11]. This is utilized in the FCS setup, as explained in following chapter. Other labels used were GFP, which is not quite as suited to the laser used here, and the externally applied TRIT-C.

## Chapter 3

# Experimental setup and methods

### 3.1 Fluorescence Correlation Spectroscopy

As already mentioned, for autocorrelation to give precise results the laser focus inside the sample needs to be very small, and we must be able to accurately measure the fluorescent decays. This can be achieved with the setup shown in Fig.3.1. The elements of the setup are explained next

#### 3.1.1 Setup

The lightsource used is a 532nm green Nd:Yag laser with a power of 5mW and a beam diameter of 0.36mm. In order for the laserbeam to properly fill the back of the objective which has a 7.2mm diameter, it needs to be widened by a factor of  $7.2\text{mm}/0.36\text{mm} = 20$ , which is achieved using two lenses in succession with a ratio of focal lengths = 20. In our setup these are 5mm and 100mm focal lengths.

Next the light travels through one of five optical density filters (OD1-OD5), which allow us to adjust the power of the laser. In our experiments only OD1 and OD2 were used, reducing the laser power to 0.5mw or 0.05mw respectively. This reduces bleaching of the fluorophores.

Next the light is reflected by a dichromatic mirror which reflects light of wavelengths shorter than 537nm and transmits light of wavelengths higher than 537nm. The light then enters the objective and is strongly focused into the sample. Two different objectives were used: An airobjective with 40X magnification and a working distance of 2.15mm - 2.89mm, and an oil emersion objective with an 60X magnification and a working distance of 0.100mm. With the oil emersion objective, a drop of oil is placed between the objective and the coverglass. The high refractive index of the oil creates a greater light collection.

When the fluorophores in the bacterial cell membranes are hit by the laser, these are excited into a higher energy level followed by an immediate decay releasing

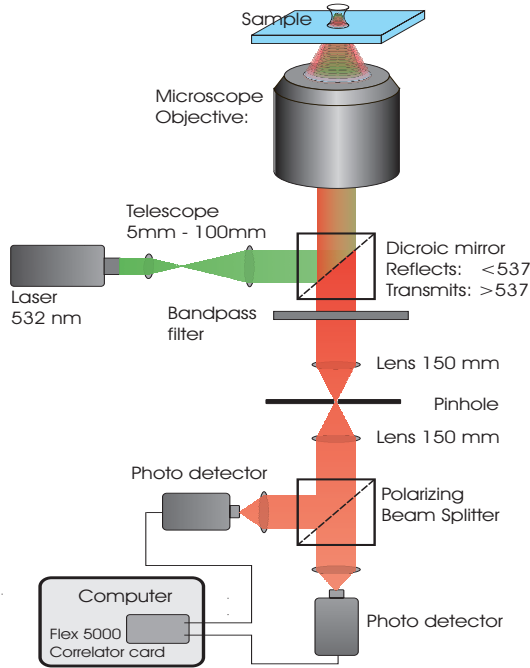


Figure 3.1: The FCS setup

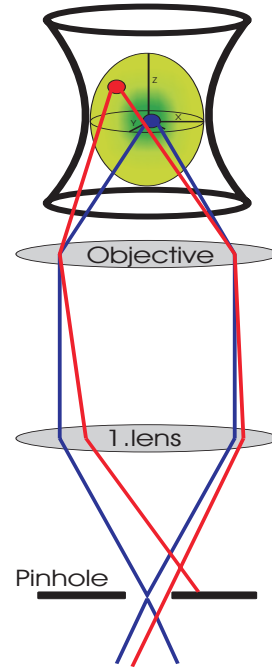


Figure 3.2: The principle of the pinhole

photons of wavelengths higher than 532nm, as covered in Sec.2.3. Some of these then re-enter the objective and are transmitted back towards the dichromatic mirror. The high wavelength of the fluorescent signal allows it to be transmitted through the mirror instead of reflected.

To further filter the signal to be registered, the light passes through bandpass filters which cut off the background signal originating from the Raman scattering of the water in the sample. The bandpass filters furthermore block the residual reflected light from the laser.

The focal plane of the objective, is not the only part of the sample where the laser light causes excitation to take place. The intensity profile of the laser light is Gaussian in three dimensions, and in order to detect only fluorescence signals originating near the focal plane where the intensity is highest, we use a pinhole (Fig.3.2). Light reaching the first pinhole lens from the center of the focal plane of the sample, will travel in rays parallel to the axis connecting the lenses, and is thereby focused exactly on the pinhole. The further from the focal plane center, the less parallel the light is when it reaches the pinhole lens and it is not allowed through. Using a  $100\mu\text{m}$  pinhole creates a ellipsoidal detection volume of approximately  $1\mu\text{m} \times 3\mu\text{m}$ .

The registration of the intensity signal takes place in the two avalanche photo diodes which allow single photon registration. Before entering the detectors, the light is split into parallel and perpendicularly polarized light by the polarizing

beam splitter. The two signals then proceed to be autocorrelated using a Flex 5000 correlator card, capable of distinguishing timeshifts down to 12.5ns. The signal could also be counted by a counter card with a time resolution of  $10\mu s$ , a measurement known as a single trace. For further detail of the setup see [7]

## 3.2 Using rhodamine to determine focal dimensions

As an important part of the experimental procedure, the FCS needs to be calibrated using a sample with a known diffusion coefficient  $D_\tau$ , before the actual experiments begin. This is done in order to determine the radius of the detection volume, having one less unknown parameter. We have used rhodamine 6G (R6G) with  $D_\tau = 3 \cdot 10^{-6} \frac{cm^2}{s}$  at 296K. Rhodamine being much smaller than the focus can be considered a point-like fluorophore diffusing freely in 3 dimensions, so the correlation curve obtained from a measurement should be fitted using Eq.2.15. Normally this would mean fitting to 3 parameters ( $\langle N \rangle$ ,  $\tau_D$  and  $r_0$ ), but knowing  $D_\tau$  for R6G however, it is possible to substitute  $\tau_D = \frac{r_0^2}{4D_\tau}$  which yields:

$$G(\tau) = \frac{1}{\langle N \rangle} \cdot \left( \frac{1}{1 + \frac{\tau}{\tau_D}} \right) \cdot \left( \frac{1}{\sqrt{1 + \frac{r_0^2 \tau}{z_0^2 \tau_D}}} \right) = \frac{1}{\langle N \rangle} \cdot \left( \frac{1}{1 + \frac{4D_\tau \tau}{r_0^2}} \right) \cdot \left( \frac{1}{\sqrt{1 + \frac{4D_\tau \tau}{z_0^2}}} \right) \quad (3.1)$$

This has only  $\langle N \rangle$  and  $\tau_D$  as fitting variables. The value for  $\tau_D$  is then used to calculate  $r_0$ , which is saved and used for the radius in all the experiments conducted afterwards. A 10nM R6G solution is used, and before measurement it is submitted to a flow of oxygen which acts as a quencher of the phosphorescence mentioned in Sec.2.3.

## 3.3 Growing and preparing bacteria

Several considerations need to be taken into account, when devising a protocol for bacterial growth and handling, for motility studies like the ones we are conducting. There are both issues of concentration and access to sufficient nutrients, as well as issues ensuring that minimum damage is inflicted on the flagellar machinery.

### 3.3.1 Bacterial protocol

The basis protocol we followed during our experiments is described here. Standard LB media with tetracycline was used as growth media, the tetracycline was added to inhibit contamination of other bacteria. Approximately 20 ml of LB media in a growth beaker was inoculated with E.coli XL1 DsRed using a sterile

wooden stick. The beaker was then left in a shaking incubator for 20-24 hours at  $37^{\circ}\text{C}$ . After a time of adaptation to the new media, the growth enters the log phase with exponential growth, where *E.coli* divides approximately every 20 min. Gradually the growth rate lessens, and after 20-24 hours the bacteria have entered a steady state with constant concentration, with equal amounts of bacteria dying and multiplying. At this time, a density in the order of  $10^8 - 10^9 \text{ml}^{-1}$  can be expected.

After this time, 0.3ml of the overnight stock is transferred to 9ml of fresh LB media, thus supplying new nutrients, and left in the shaking incubator for about 3 hours. After the 3 hours the beaker is transferred to an oven fixed at  $37^{\circ}\text{C}$ , from where samples are prepared.

To prepare a sample for measurement, 1ml of stock is put in a microcuvette and centrifuged at 5000rpm for 10min. The supernatant is removed, and  $400\mu\text{l}$  of fresh LB media is put into the microcuvette. The pellet is resuspended in the new media using a minishaker. To allow the bacteria to recover from the shaking, the sample is left in the oven for 45 min afterwards. The  $400\mu\text{l}$  are then transferred to a chambered coverglass and measurements are performed. At the time of measurement density is expected to be about  $10^9 \text{ml}^{-1}$ .

A smaller series of experiments were performed on a different strand of *E.coli*. This strand was simply not equipped with the vector carrying information for the production of red fluorescent protein, but was otherwise identical to the other strand. In order to detect it, we labelled it externally using TRIT-C. The same bacterial protocol was used, with the only difference being the addition of  $5\mu\text{l}$   $0.404\mu\text{M}$  TRIT-C to the microcuvette containing the 1 ml sample going into the centrifuge.

### 3.3.2 Adjusting the conditions

For experiments involving changing of the pH, the following procedure was followed. pH was changed directly in the chambered coverglass immediately prior to measurement. We used HCl and NaOH to change the pH, which was measured on a standard pH meter.

To control the temperature during measurements, a heat bath connected to a heating hood fitting around the measuring chamber was used. Temperature was adjusted on the heat bath, but the actual temperature in the chamber was measured directly with a thermometer.

A final series of measurements were conducted at room temperature without the heat bath. The bacteria that we prepared for this study were kept at room temperature for 4 hours after the 3 hours growth. Preparation of samples was the same, only the oven was not used.

### 3.4 General considerations

A number of considerations regarding the experimental procedures and setup are worth keeping in mind when analyzing the results.

A very important issue is the phenomenon of bacterial adhesion. Several experiments have documented that bacteria, including *E.coli*, in close proximity to a planar surface such as a coverslip, will not only have their freedom of movement restricted by the surface, but also experience adhesive forces keeping it near the surface, or even causing it to stick [10].

To minimize this effect, it is very important that our detection volume is well inside the chamber and away from the surfaces. The initial setup for the experiment involved an oil emersion objective with a working distance of only  $100\mu m$ . With the air objective with its long working distance, we hope to have minimized adhesion.

Generally working with living and constantly multiplying test subjects, makes it very difficult to achieve high consistency in the experiments. Small differences in growing times and growth conditions from experiment to experiment can influence the reproducibility of results from day to day. It is also the case when doing a full pH or temperature series over several hours. Concentrations are inevitably not constant. Even within the same measurement of 10-20 min conditions change, both with regards to concentration and pH, since the byproducts of bacterial metabolism also effect pH.

Another technical aspect concerning the measurements, is the presence of temperature gradients in the sample chamber. Since the heat bath only applies heat to the chamber from the top by way of the hood, a small gradient form down through the liquid. The temperature difference from the top of the liquid to the bottom is usually about  $2^{\circ}C$ . How much convection this gradient gives rise to, is hard to tell, but due to the sizes of particles and detection volumes, even small currents might influence the results.

# Chapter 4

## Results

The results presented here, are the condensed results of a number of measurements of E.coli under different conditions of temperature and pH. Measurements have involved two different objectives and 3 different E.coli strands each labelled differently.

### 4.1 Rhodamine measurements

Before each series of measurements, it is necessary to conduct a FCS measurement on a 23°C 10nM solution of Rhodamine6G in order to determine the focal radius of the day. By adjusting the pinhole, and the objective distance from the sample, the setup is optimized to give the smallest focal radius  $r_0$ , as well as a high fluorescence signal per fluorophore, when fitting the correlation data with Eq3.1. The value obtained for the radius is kept, and used for the fitting of the later obtained bacterial correlation data. All rhodamine recordings were conducted with optical density filter OD1 and a pinhole of 100 $\mu$ m.

A typical Rhodamine correlation curve recorded by the air objective, is seen in Fig.4.1. It has been fitted using Eq.3.1, with the radius  $r_0$  obtained as a coefficient. For the fit,  $z_0$  of the focus is kept fixed at 3000nm. The right boundary for the fit is set where the correlation value is 1 and approximately constant. The left boundary is set on the first plateau before the curve drops, but not including the noise from the faster phosphorescence.

We see that the major event on the correlation curve happens for values of  $\tau \in [10^{-5}s; 10^{-3}s]$ . The radius obtained from the fit was 584nm. From this, the mean diffusion time  $\tau_D$  was calculated to  $2.8 \cdot 10^{-4}s$ . The variation in  $r_0$  from day to day was found to be in the order 60nm, giving us radiuses from 550nm to 610nm, but with the most typical being around 570nm.

Also worth noticing, is the shape of the Rhodamine correlation curve. The drop is fairly smooth and extended, spanning over almost 3 orders of magnitude, which is typical of pure diffusion.

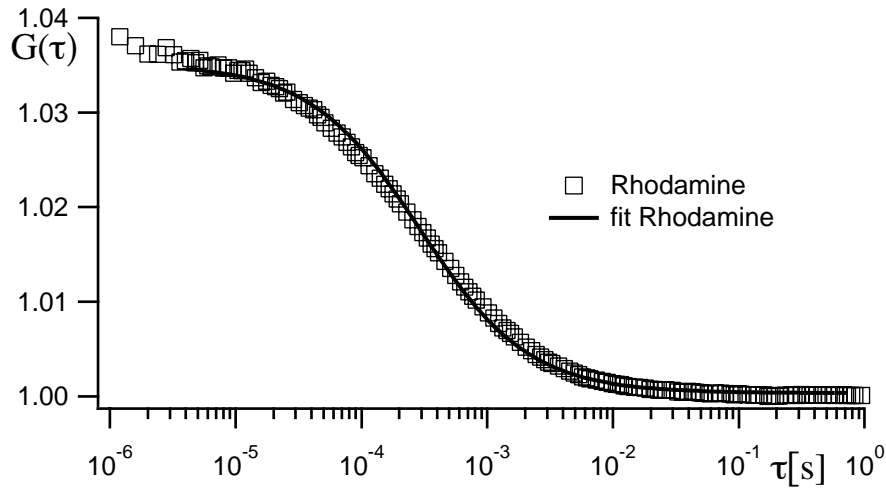


Figure 4.1: Fitted rhodamine correlation curve. 23°C, 10nM, OD1, pinhole 100  $\mu\text{m}$

## 4.2 Single trace measurements and intensity pattern

In order to visualize an actual passage of an E.coli, we recorded a single trace. Intensity data is also obtained from a normal correlation measurement, but this is the accumulated photon hits during an entire second, and does not give a good time resolution of a passage.

The single trace was recorded at 35°C and with a pH of about 6.5 using Ecoli labelled with DsRed. The binning size was set to 60 $\mu\text{s}$  and the run time to 5 min

Fig.4.2 and Fig.4.3 shows the results of the single trace. Fig.4.2 is a slightly smoothed graph of the entire 5 min run, while Fig.4.3 shows the smoothed data

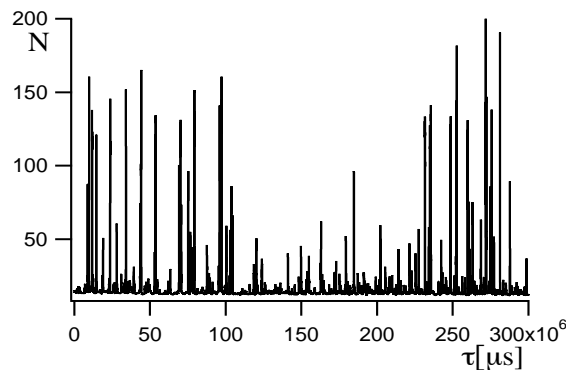


Figure 4.2: smoothed 5 min. single trace. DsRed, 35°C, pH6.5. N is the number of photon hits during a bin of 60 $\mu\text{s}$

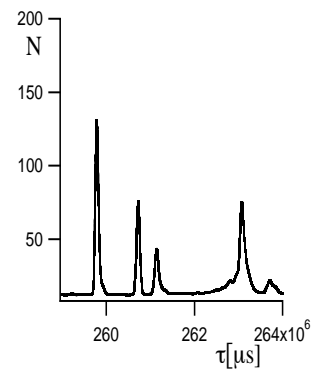


Figure 4.3: 5 second subsection of data

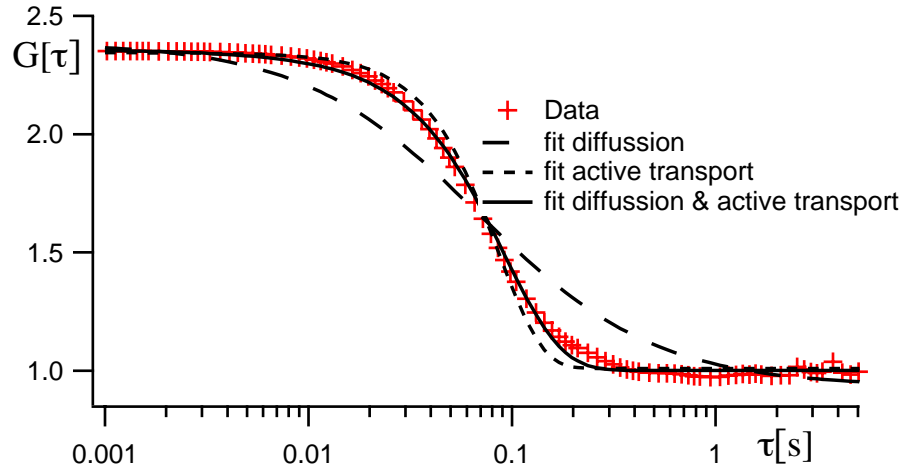


Figure 4.4: Fitting of a bacterial correlation curve. DsRed, 35°C, pH 6.5

from a 5 second subsection. It is evident from these figures, that events do in fact occur, and also that the events differ in size and length. With a simple background measurement of LB media without bacteria not producing any events like these (not shown), they must be ascribed to passing bacteria.

Doing a crude measurement of the lengths of the individual peaks of a 30 second subsection of the 5 min run, reveals an average peak width of approximately 0.17s. Assuming the bacteria have evenly distributed fluorophores, different passage times are probably due to different trajectories through the focus. The differences in amplitude for the passages comes from the Gaussian intensity profile, with high peaks corresponding to passages near the focal plane. Of course there will also be some variation between the individual bacterial sizes and swimming speeds.

Using the strand of E.coli externally labelled with TRIT-C revealed a similar pattern of events, which could also be obtained with E.coli modified to produce Green Fluorescent Protein GFP instead of DsRed.

### 4.3 Fitting procedures and data editing

In Sec.2.2.3 we arrived at Eq.2.19 for the correlation function with active transport taken into account. Fig.4.4 shows a typical correlation curve for a bacterial measurement, as well as fits using Eq.2.15, Eq.2.20 and Eq.2.19 for pure diffusion, pure active transport and the combined correlation function of the two, respectively. The figure reveals that using the combined correlation function produces the most accurate fit, very similar to that of pure active transport. The pure diffusion equation is seen to match the data very poorly when fitted. This tells us that

active transport plays the major role in the motility of our bacteria, and therefore that  $\tau_A$  obviously is the coefficient of interest, when comparing the motility of swimming bacteria.

All data have been edited to make comparisons easier and to cut away irrelevant information. The raw unedited data is based on Eq.2.9 with correlation values starting above one and moving towards one as correlation disappears. By subtracting one from the data for each correlation curve and dividing by the highest value, all curves have been normalized to 1. In addition, correlation times  $\tau < 10^{-3}s$  and  $\tau > 10^1s$  have been cut away, since on these timescales the correlation is either constant or stemming from sources other than bacteria<sup>1</sup>. All bacterial data, from here on, are fitted to the correlation function containing both the diffusion and active transport as given by Eq.2.19.

## 4.4 Temperature dependence

For the series of measurements conducted concerning the temperature dependence of E.coli motility, the following procedure was followed.

Prior to a given temperature measurement, the temperature of the heat bath was adjusted by measuring the exact temperature in a calibration sample. Depending on the temperature this usually meant setting the heat bath  $2^\circ C - 4^\circ C$  above the wanted temperature. Due to the presence of temperature gradients as mentioned in Sec.3.4, temperature was always measured in the middle of the chamber. Preparation of the test sample followed the protocol in Sec.3.3.1. When the desired temperature was obtained, usually after a few minutes, measurements began. All measurements were 5 min runs, and depending on conditions, two or three were obtained for each temperature. DsRed was used for the experiment. Temperature measurements were made from  $30^\circ C$  to  $41^\circ C$ . The signal from each of the photodetectors was correlated with itself with a resolution of  $12.5ns$ . In order to reduce variation originating from the fact that we used living testobjects, a full series was conducted in the same day working on the same overnight preparation of bacteria.

Fig.4.5 and Fig.4.6 shows the correlation data and  $\tau_A$  values from a series of temperature measurements. In Fig.4.5 each temperature measurement is represented by a single correlation curve. Fig.4.6 contains the fit values of  $\tau_A$  for all correlation curves obtained from each temperature. The correlation curves are clearly displaced over a wide range of  $\tau$  values, indicating different active transport times, as explicitly seen on Fig.4.6. The shape of the correlation curves are identical and resembles the correlation profile of active transport on Fig.4.4, which also is evident from the  $\tau_A$  and  $\tau_D$  ratios from the two profiles. Based on these data there does not seem to be any clear connection between the temperature and

---

<sup>1</sup>The slowly falling signal caused by bleaching, would for example result in a small correlation on large timescales, whereas phosphorescence correlate on very small timescales

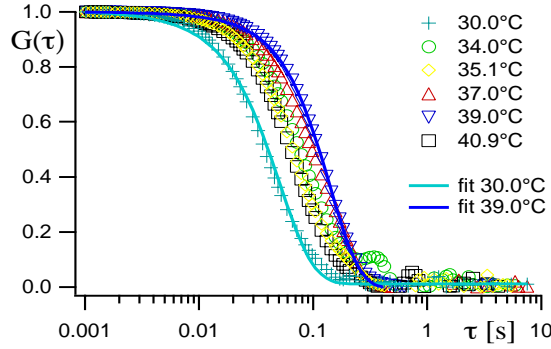
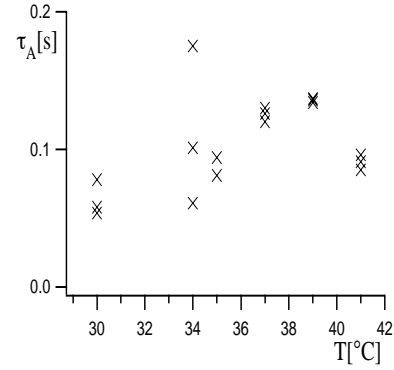


Figure 4.5: Temperature dependence. DsRed, pH6.5

Figure 4.6: Scattering of  $\tau_A$  with temperature

the displacement of the correlation profiles and their corresponding  $\tau_A$  values.

Previous motility studies on temperature dependence suggest an increase in motility with temperature in the order of 15 – 20% when increasing the temperature from 30°C to 40°C [13]. An increase that is probably mostly due to the viscosity decrease with temperature, although a change in tumble frequency with temperature also affected swimming speed. For water, the viscosity drops from 0.798 to 0.653 centipoise when the temperature increases from 30°C to 40°C, corresponding to an 18% drop.

Given the quality of our measurements, with the average scattering of  $\tau_A$  in Fig.4.6 amounting to approximately 25%, a temperature dependency, in the order of the above mentioned, would be hard to confirm. Especially taking the relative low number of measurements into account.

## 4.5 pH dependence

A series of measurements seeking to investigate bacterial motility dependence on pH was also conducted. The growth of the bacteria and changing of the pH followed the protocol in Sec.3.3. pH was changed immediately prior to a recording. Measurements were made for pH4 to pH9, at a fixed temperature of 35°C in the middle of the measuring chamber. The pH values cited in the results, are the values measured before a recording. The pH was also measured after the recording and was generally found to have dropped, by up to 0.3pH. After a few minutes to attain the 31°C, two 5 min runs were recorded for each sample. Again DsRed was used in the experiment

Fig.4.7 and Fig.4.8 are the correlation curves and their corresponding  $\tau_A$  values obtained from this experiment. The shape of the correlation curves are seemingly not affected by the changing of pH. As seen for temperature measurements, the curves are however also here spread over different transport times. A connection

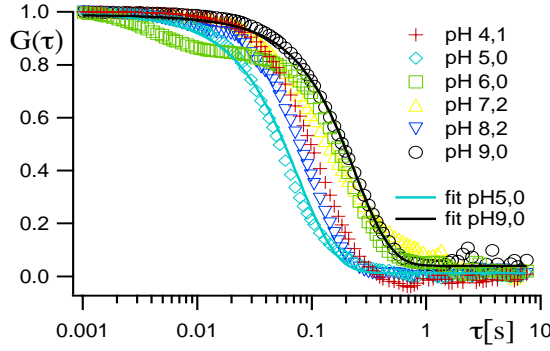
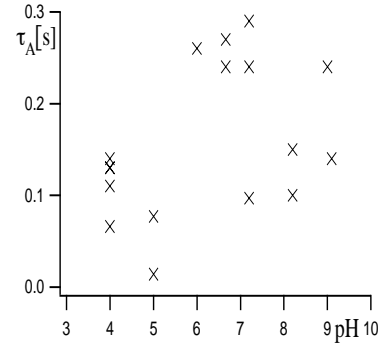


Figure 4.7: pH dependence. DsRed, 35°C

Figure 4.8: Scattering of  $\tau_A$  with pH

between pH and active transport time does not seem to exist based on our data.

Previous studies conducted on pH dependent motility have seen only very little connection between pH and swimming speeds [15][14]. These studies have found maximum swimming speeds at around pH 6.5, with speed slowly falling off to either side. In one of these studies [14], the pH range investigated went from pH 5 to pH 8, with measured swimming speeds varying from about  $20 \frac{\mu m}{s}$  at pH 5 and pH 8 to about  $25 \frac{\mu m}{s}$  at pH 6.5. The scattering of our pH data is considerable, and once again prohibits the detection of a dependency in this order of magnitude.

Recording swimming speeds in the order of  $20 \frac{\mu m}{s}$  to  $30 \frac{\mu m}{s}$  would correspond to measuring values of  $\tau_A$  in the range of 0.040s to 0.060s, given a diameter of the focus of 1200nm. As seen on Fig4.8, we seem to be recording  $\tau_A$  values that are a little to slow, similar to that seen on the single trace measurement. However taking the size effect into account as mentioned in Sec.2.2.3, as it should be whenever mentioning absolute transport times, would mean subtracting up to 0.040s from our recorded values which would bring us closer to the known regime. Referring to swimming speeds, means the combination of active transport and diffusion. With active transport being dominant however, diffusional effects are close to negligible.

The above mentioned study was conducted at 23°C, whereas the data for Fig.4.7 and Fig.4.8 was recorded at 35°C. A pH dependency experiment was done at 23°C. For this experiment the protocol in Sec.3.3.1 was followed, allowing the bacteria 4 hours to adapt to room temperature before measuring. pH was changed and measured directly prior to measurement and again afterwards. Again pH was found to have dropped slightly. No heat bath and heating hood was used in the experiment. For each pH, two or three runs of 2 or 5 min were recorded.

Fig.4.9 shows the results of the experiment. It is seen that the results do not correspond with neither the results obtained at 35°C, nor with the results of the studies referred to above. Comparing Fig.4.9 to Fig.4.7 and Fig.4.5 it is seen that the correlation curves recorded at room temperature are generally slightly faster than both the pH curves at 35°C and the temperature dependence curves.

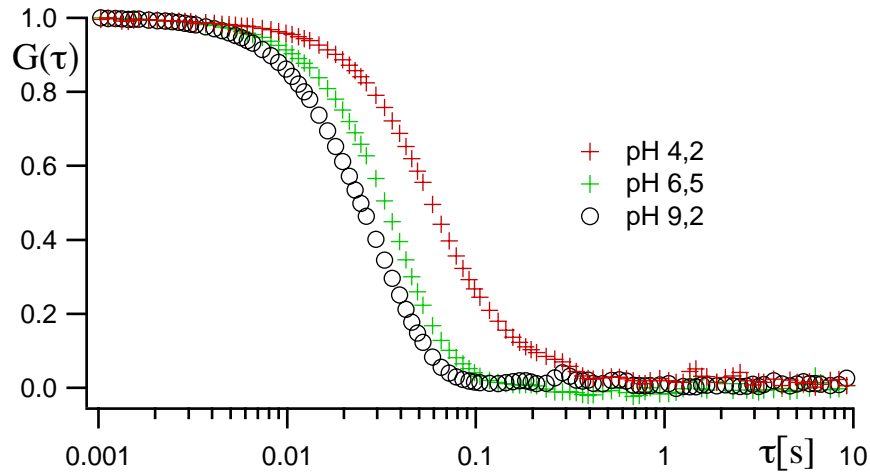


Figure 4.9: pH dependence. DsRed, 23°C

## 4.6 Adhesion & dead bacteria

With the high degree of variation presented in the two dependency experiments, it has proved impossible to confirm the connections established in previous studies. With the accuracy of our methods, we are apparently not able to identify dependencies on the relative small scale seen in these two experiments. By drawing on data from our initial experimental approach where an oil objective was used instead of the air objective, we are able to investigate motility data for two very different situations. As mentioned in Sec.3.4, the short working distance of the oil objective, only permits us to obtain data at the very bottom of the measuring chamber, where a high degree of adhesion is known to take place.

Fig.4.10 presents data from oil objective recordings and data from air objective recordings, obtained under similar conditions. It is seen from the correlation curves, that a high degree of variation also exist in the oil objective data, but that the center of the variation seem to be shifted towards higher active transport times, as would be expected for bacteria near to a surface, being restricted to two dimensional movement, or sticking. Comparing the shapes of the two groups of curves, reveal no obvious difference, indicating that active transport is still dominant in the movement near surfaces. The average active transport time  $\tau_A$  for air objective correlation data is around 0.1s while the oil objective reveal values around 1s. Taking the oil objective's smaller radius into account ( $\frac{2}{3}$  times the air objective's radius) the variation in actual swimming speeds between bacteria in solution and close to surfaces, would be slightly smaller.

Apparently, changes on this magnitude are detected by our FCS setup. The existence of scatter in the oil objective data on the same order as the scatter obtained in the air objective data, suggests that both types of measurements are

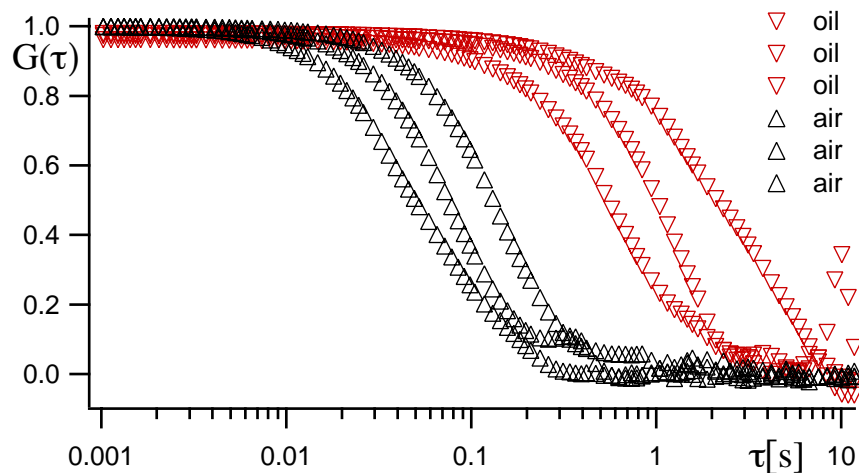


Figure 4.10: Correlation curves from oil objective recordings and air objective recordings. DsRed,  $35^{\circ}\text{C}$

influenced by the same sources of error, or at least sources of error of the same magnitude.

Fig.4.11 shows the correlation profiles of dead bacteria along with those of typical living bacteria under standard conditions, in addition to a rhodamine curve. Bacteria were killed by adding a small amount of  $\text{NaN}_3$ . All data are recorded with the air objective.

It is noticed from the figure that the transport times are different depending on whether the bacteria are dead or alive. This corresponds to what would be expected. The average active transport time for living bacteria at standard pH and a temperature of  $35^{\circ}\text{C}$  is approximately  $0.1\text{s}$  whereas those for the dead bacteria are substantially larger, in the order of  $1\text{s}$ . Comparing the profile shapes, seem to indicate a slight tendency for the dead bacteria to assume a more diffusion like shape than the living bacteria. This is supported by the fitting coefficients, which reveals that the ratio of  $\tau_A$  and  $\tau_D$  is shifted slightly towards diffusion compared to that of the living bacteria.

We would expect purely diffusing bacteria to produce correlation profiles with a shape much more resembling that of rhodamine.

It should be said, that generally the recordings on dead bacteria often gave peculiar intensity signals and correlation profiles. We saw large not well defined peaks, which could be interpreted as bundles of bacteria sticking together.

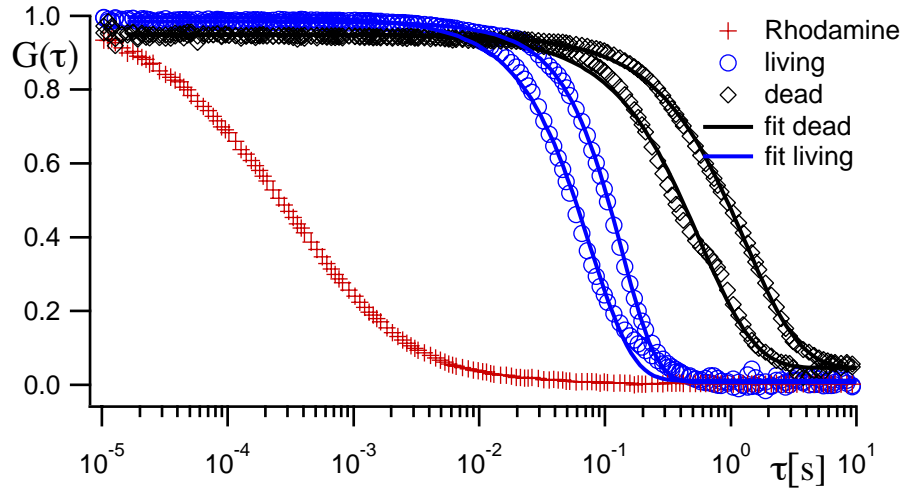


Figure 4.11: Correlation profiles for rhodamine, living bacteria and dead bacteria. DsRed, 35°C, pH 6.5

## 4.7 Errors and uncertainties

The existence of the noticeable amount of scatter in the data, and the inability to produce correlation curves with distinct diffusive character of dead bacteria, suggest the presence of artifacts in our experiments. Possible origins of such artifacts are discussed in the following.

One likely source of error, is that of convection. As mentioned in the theory section, the means of heating our sample could give rise to a not negligible convection, especially since the sample was free to evaporate during measurements. The measurement of actual temperature gradients within the sample, states that convection indeed must have occurred. Convection could partially help to explain a number of the observed phenomena. The dead bacteria's correlation curve would indeed be more active-like than the expected diffusion-like, in the presence of convection in the same order of magnitude as the transport times. Such a convection would not affect faster moving objects, which is consistent with our measurements of rhodamine, that is definitely recorded as diffusing.

The high degree of scatter can also be explained by convection. Since we had no way to make sure that each measurement was conducted the exact same place in the measuring chamber, the convective cells forming in the presence of temperature gradients, is likely to have had varying directions from measurement to measurement. Even tiny displacement of the focus could cause it to enter a place with a different flow pattern.

In addition it can not be ruled out, that a convection slowly settling to a steady state could be the reason behind the general trend, that the first correlation curve

obtained was seen to be faster than the consecutive ones.

It should be fairly easy to minimize the presence of convection by utilizing a setup combining a long working distance with the ability to heat the sample from the bottom. A water emersion objective would probably be suited for this. Unfortunately mechanical defects did not allow us to investigate this.

The measurement in a series would last over several hours, and thereby result in an increasing concentration of bacteria. This should not give cause to changes in the bacterial movement as they would still be sparsely spread throughout the sample. Another effect of increased concentration however, is its effect on the transparency of the sample. A reduced transparency acts to absorb more of the laser light before it reaches the focal plane, resulting in a lower fluorescent intensity and a lower signal to noise ratio. It should therefore be taken into account when conducting experiments, however this is easily compensated by diluting the sample, and was not a problem.

Due to the high degree of scatter in our data, and the lack of dependency on temperature and pH in our experiments, it has not seemed meaningful to present the data with margins of uncertainty.

## 4.8 Conclusion

Up until now fluorescence correlation spectroscopy has been an untried approach to the study of bacterial motility. Our investigation of its application in this field, although not conclusive, indicates that there are definitely perspectives.

We have shown that a standard FCS setup is able to detect and correlate intensity fluctuations in a solution containing labelled E.coli. It has also been shown, that the means of labelling, external or genetic, do not influence the obtained results. Furthermore, both an air objective with a relatively large detection volume and an more focused oil objective have been shown to produce correlation results. In addition to this, results for both freely moving E.coli as well as bacteria experiencing the phenomena of bacterial adhesion, has been seen. Dead bacteria has also been shown to exhibit movement distinctly different from that of living bacteria. This reveals that FCS is capable of conducting experiments on several aspects of bacterial movement.

On smaller timescales however, the scattering of our results did not allow us to identify motility dependencies like those expected for pH and temperature, perhaps mainly due to the presence of convection. Overall though, the active transport times obtained in the two experiments were found to correspond to swimming speeds in the expected order of magnitude. This was especially shown to be true, when taking the size effect into consideration, which indicates that such an effect does in fact influence autocorrelation.

The existence of a high degree of data scatter, as well as our inability to decisively detect diffusion profiles from dead bacteria, suggest that work remains to be done with optimizing the setup and adjusting experimental procedures, starting with the removal of convection. Theoretical issues concerning the corrections to the correlation function for large self propelled particles with multiple fluorophores, can also be the focus of further studies.

Overall it is however clear that FCS also has a potential for the study of self propelled organisms, and given it's enormous statistical advantage to other existing methods it might be the more powerful.

# Bibliography

- [1] Elson E.L., Magde D: Fluorescence Correlation Spectroscopy.I.Conceptual basis and theory. Biopolymers 13, 1-27 (1974)
- [2] Howard C. Berg: Motile Behavior of Bacteria. Article on Physics today on the web
- [3] Berg, H. C. 1971: How to track bacteria. Rev. Sci. Instrum. 42:868871.
- [4] ROLAND THAR,\* NICHOLAS BLACKBURN, AND MICHAEL KUHL: A New System for Three-Dimensional Tracking of Motile Microorganisms APPLIED AND ENVIRONMENTAL MICROBIOLOGY, May 2000, p. 22382242 Vol. 66, No. 5
- [5] Howard C. Berg: Random walks in Biology; expanded edition (1993)
- [6] Petra Schwille, Elke Haustein: Fluorescence correlation spectroscopy, a tutorial for the biophysics textbook, 2002
- [7] Agnieszka Hac: Diffusion Processes in Membranes Containing Coexisting Domains Investigated by Fluorescence Correlation Spectroscopy (2003)
- [8] H. Khler, P. Schwille, W. W. Watt, M. R. Hanson: Active protein transport through plastid tubules; velocity quantified by fluorescence correlation spectroscopy.
- [9] Konstantin Starchev, Jingwu Zhang and Jaques Buffle: Applications of Fluorescence Correlation Spectroscopy - Particle size effect. Journal of colloid and interface science 203, 189-196 (1998)
- [10] MA Vigeant and RM Ford: Interactions between motile Escherichia coli and glass in media with various ionic strengths, as observed with a three-dimensional-tracking microscope. Appl.Environ. Microbiol., Sep 1997, 3474-3479, Vol 63, No. 9
- [11] <http://www.microscopyu.com/articles/livecellimaging/fpintro.html>
- [12] <http://www.olympusmicro.com/primer/lightandcolor/fluoroexcitation.html>
- [13] KAYO MAEDA, YASUO IMAE, JUN-ICHI SHIOI, AND FUMIO OOSAWA: Effect of Temperature on Motility and Chemotaxis of Escherichia coli. JOURNAL OF BACTERIOLOGY, Sept. 1976, p. 1039-1046
- [14] Tohru Minamino, Yasuo Imae, Fumio Oosawa, Yuji Kobayashi, and Kenji Oosawa : Effect of Intracellular pH on Rotational Speed of Bacterial Flagellar Motors. JOURNAL OF BACTERIOLOGY, Feb. 2003, p. 11901194 Vol. 185, No. 4
- [15] Xiaobing Chen and Howard C. Berg: Solvent-Isotope and pH Effects on Flagellar Rotation in Escherichia coli. Biophysical Journal Volume 78 May 2000 22802284